Materials Today Bio 16 (2022) 100415

Contents lists available at ScienceDirect

Materials Today Bio

journal homepage: www.journals.elsevier.com/materials-today-bio

Co-axial fibrous scaffolds integrating with carbon fiber promote cardiac tissue regeneration post myocardial infarction

Jie Meng [a,1], Bo Xiao [b,1], Fengxin Wu [a,1], Lihong Sun [c], Bo Li [d], Wen Guo [d], Xuechun Hu [a], Xuegai Xu [a], Tao Wen [a], Jian Liu [a,**], Haiyan Xu [a,*]

[a] Department of Biomedical Engineering, Institute of Basic Medical Sciences, Chinese Academy of Medical Sciences & Peking Union Medical College, Beijing, 100005, China
[b] Department of Anesthesiology, Peking Union Medical College Hospital, Chinese Academy of Medical Science & Peking Union Medical College, Beijing, 100730, China
[c] Center for Experimental Animal Research, Institute of Basic Medical Sciences, Chinese Academy of Medical Sciences & Peking Union Medical College, Beijing, 100005, China
[d] Peking Union Medical College, Beijing, 100730, China

ARTICLE INFO

Keywords:
Conductive Scaffold
Carbon fibers
Myocardium
Regeneration
Vascularization

ABSTRACT

Myocardium is an excitable tissue with electrical conductivity and mechanical strength. In this work, carbon fibers (CFs) and co-axial fibrous mesh were integrated which combined the high modulus and excellent electrical conductivity of CFs and the fibrous and porous structures of the electrospun fibers. The scaffold was fabricated by simply integrating coaxial electrospun fibers and carbon fibers through a freeze-drying procedure. It was shown that the integration of carbon fibers have the conductivity and Young's modulus of the fibrous mesh increased significantly, meanwhile, upregulated the expression of CX43, α-actinin, RhoA of the neonatal rat primary cardiomyocytes and primary human umbilical vein endothelial cells (HUVECs), and promoted the secretion of VEGF of HUVECs. Moreover, the cardiomyocytes grown on the scaffolds increased the ability of HUVECs migration. When implanted to the injury area post myocardial infraction, the scaffolds were able to effectively enhance the tissue regeneration and new vessel formation, which rescued the heart dysfunction induced by the myocardial infraction, evidenced by the results of echocardiography and histochemical analysis. In conclusion, the composite scaffolds could promote the myocardium regeneration and function's recovery by enhancing cardiomyocytes maturation and angiogenesis and establishing the crosstalk between the cardiomyocytes and the vascular endothelial cells.

1. Introduction

Heart tissue is highly electroactive elastic and sensitive to electric signal to complete the cardiac myocytes relaxation and contraction [1]. After acute myocardial infarction (M.I.) occurred, the injured tissue could lead to progressive heart wall thinning, myocardial function maladaptation and fibrosis scar formation if proper treatments are not performed in time [2], and the scar tissue can decrease or even block the electric propagation and further induce the heart functional decompensation [3]. Therefore, to stop the progressive wall thinning and prevent the scar formation are crucial for the treatment of the post M.I. In the past decades, large amounts of endeavor have been made, which have led to great achievements with mechanism insights to the important issues [4–8], among these, applying a local patch to the surface of the infarcted ventricle represents a promising strategy that has exhibited superiority in recovering the function of damaged hearts [9].

It has been documented that the conductivity of implanted scaffolds is crucial for heart tissues besides the mechanical support as myocardium itself is electrically conductive and excitable [10]. For example, the implantation of conductive patch to the infarcted area can prevent the scar tissue of the heart wall from thinning, which is beneficial to remaining the cardiac function [11,12]; additionally, the conductive scaffolds allow rapid cell-cell communications and enable the regenerated tissues to acquire more physiological functions [13]. Therefore, an ideal novel conductive scaffold should be able to transduce physiological electrical signals, support the synchronous contraction [14,15] and promote

* Corresponding author.
** Corresponding author.
E-mail addresses: liujian@ibms.pumc.edu.cn (J. Liu), xuhy@pumc.edu.cn (H. Xu).
[1] These authors contributed equally to this work.

https://doi.org/10.1016/j.mtbio.2022.100415
Received 29 June 2022; Received in revised form 15 August 2022; Accepted 30 August 2022
Available online xxxx

neovascularization [16] providing nutrients and oxygen to cardiomyocytes regeneration. Up to date, there have been a variety of scaffolds under intensively investigations, mainly including hydrogels [11,13,17], fibrous or porous meshes [18–20], composites integrating conductive inorganic nanoparticles [21,22] or conductive polymers [23,24], and several comprehensive review articles have summarized the research progresses [10,25]. Nevertheless, there is still a large space in the fabrication of 3D conductive scaffolds to guide better regeneration of the myocardium post M.I. Although electrospun fibrous scaffolds can well mimic the structures or components of extracellular matrices, they are usually in film forms, and it would be more ideal for hydrogels or porous polymer materials to acquire not only ECM-like microstructures but also sufficient modulus and conductivity by more flexible fabrication ways.

Carbon fibers (CFs) are synthetic fibers made especially by carbonizing acrylic fibers at high temperatures, featured with very high modulus and conductivity as well as very specific weight, the carbon content usually can be more than 93%. Therefore, CFs can bring elastic modulus, conductivity, and high carbon content to substrates. Different from conductive nanomaterials, the diameter of CFs can be precisely controlled, usually 7 μm that is close to the diameter of purkinje fibers transducing electrical signals in myocardial tissue. So far, CFs have been widely applied as reinforcing material for polymer matrix composites in industries [26]. In biomedical fields, CFs have been explored only in the implantable bone grafts and hip joint [27,28], however, rarely applied to tissue engineering scaffolds yet. We previously reported that CFs largely increased the conductivity and stiffness of polyvinyl alcohol (PVA), significantly enhancing the maturation and electrophysiological function of neonatal rat cardiomyocytes (NRCMs) in vitro [29] and indicating CFs' promising potentials in the guidance of heart tissue regeneration. In this work, we integrated CFs with coaxial electrospun fibers of PLA@Gelatin, aiming to combine the excellent conductivity, high modulus and biocompatibility with the fibrous and porous structures. We showed that the resulting composite scaffold (PLA@Gel/CF) obtained the conductivity close to that of natural heart tissue and largely increased compress modulus, which not only accelerated the cardiomyocytes maturation and connection, but also increased the angiogenesis and crosstalk between cardiomyocytes and vascular endothelial cells. The implantation of PLA@Gel/CF significantly promoted the cardiac tissue regeneration and function recovery *in vivo* post M.I.

2. Materials and methods

2.1. Materials, cell and animal

Poly lactide (PLA) with the average molecular weight of 80 kD was purchased from Chang Chun Sino Biomaterial Co., Ltd, Changchun, China. Type A gelatin was purchased from Sigma-Aldrich Co., Ltd. The polyacrylonitrile (PAN)-based carbon fibers (CFs) of 7 μm in diameters was produced by the National Carbon Fiber Engineering Technology Center, Beijing University of Chemical Technology.

Adult male Sprague-Dawley (SD) rats (200 g–250 g) were purchased from Beijing Huautong Experimental Animal Technology Co., Ltd., China, and the experimental protocol was approved by the Animal Care and Use Committee of the Basic Medical Sciences, Chinese Academy of Medical Sciences. Neonatal rat cardiomyocytes (NRCMs) were isolated from 1~3-day-old SD rats [30] and cultured in high glucose Dulbecco's Modified Eagle's Medium (DMEM, Gibco) supplemented with 10% fetal bovine serum (FBS), 1% penicillin/streptomycin and 1% 5-bromodeoxyuridine (5-BrdU) at 37 °C and 5% CO_2. Primary human umbilical vein endothelial cells (HUVECs) were purchased from ScienCell Research Laboratories (San Diego, CA), and cultured in endothelial cell medium with growth supplements provided by the company.

2.2. Preparation and characterization of scaffolds

Electrospun nanofibers were prepared by coaxial electrospinning, PLA dissolved in trifluoroethanol (TFEA) at 20% (w/v) as the core and gelatin in TFEA at 10% (w/v) as the shell. The electrospinning condition was set as following: voltage was 20 kV, distance was 15 cm, and the flow rate was controlled at 1 mL/h. The collected nanofibrous film (2 g) was cut into small pieces and dispersed in 100 mL tert-butanol by homogenizing (IKA T18) for 35 min at 13,000 rpm. CFs cut into 2 cm were dispersed in tert-butanol. and added to the nanofibers' dispersion. The mixture was homogenized for 5 min. Next, the mixture containing CFs of 1.0 mg/mL (PLA@Gel/CF1), 3.0 mg/mL (PLA@Gel/CF3), and 5.0 mg/mL (PLA@Gel/CF5) was vacuumed to remove the solvent, transferred into cell culture dishes and frozen-dried for 24 h. The PLA@Gel was prepared as control. All the materials were then cross-linked by glutaraldehyde in ethanol (5%) for 10 min, washed with 0.75% glycine solutions for 5 times, and then was frozen-dried to obtain 3D scaffolds.

The electrospun films were observed by scanning electron microscopy (SEM, Gemini SEM 300). To examine the core-shell structure, gold nanoparticles were added in the PLA solution and the resulting fibers were observed by transmission electron microscopy (TEM, 1400 plus). The morphology of the electrospun fibers was observed by SEM. The electrical conductivity of scaffolds was measured by using four-point probe technique (Mitsubishi Chemical Loresta-GX MCP-T700, Japan). The scaffolds of 10 mm × 6 mm were prepared for compression tests. The compression strain-stress curves were measured with both dry scaffolds and water swelled scaffolds at strain rate of 3 mm/min at room temperature (Instron 5843, 1000-N loaded sensor). The densities (ρ) of the scaffolds were calculated by the following equation:

$$\rho = m/v.$$

where m was the mass of the scaffold, and v was the volume of the scaffold.

The water absorption property of the scaffolds was tested by following steps and displayed as R_a [31]. First, dry scaffolds were weighed (W_0). Then, the scaffolds were placed in a dish containing distilled water and were taken out and weighed (W_1) at 5, 15, 30, 60, and 120 min. The Ra was calculated by the equation of $R_a=(W_1–W_0)/W_0$.

The porosity (P) of the scaffolds was measured by using the ethanol adsorption approach. In brief, the dry scaffolds were weighted (W_0) and volume was measured (V_0). Then the scaffolds were immersed in ethanol for 2 h and weighted (W_e). The porosity of each scaffolds was calculated by the equation of $P=(W_e\text{-}W_0)/(V_0 \times 0.79) \times 100\%$.

2.3. Cell viability and cytokine assay

NRCMs or HUVECs of 1×10^4 cells/well were seeded on PLA@Gel and PLA@Gel/CF3 for 5 days. The cell viability was measured using cell counting kit 8 (CCK-8; Dojindo). NRCMs or HUVECs of 8×10^5 were seeded on PLA@Gel and PLA@Gel/CF3 in a 6-well culture plate, the supernatants were collected at 48-h. Vascular endothelial growth factor (VEGF) expression of NRCMs and plasminogen activator inhibitor-1 (PAI-1) expression of HUVECs were measured by ELISA kit (Neobioscience, China).

2.4. Western blot

NRCMs or HUVECs of 1×10^6 were seeded on PLA@Gel and PLA@Gel/CF3 in 6-well culture plates. After incubation, the cells were washed with phosphate buffered saline (PBS, pH = 7.4) and lysed in RIPA buffer and the protein concentration was determined with Pierce BCA Protein Assay Kit (Thermo Fisher Scientific). Primary antibodies of anti-connexin 43 (Cx43, CST), anti-Sarcomeric α-actinin (Abcam), anti-CD31

(Abcam), anti-VE-cadherin (Abcam), anti-RhoA (CST), anti-hypoxia-inducible factor 1α (HIF-1α, CST) and anti β-actin (CST) were applied. The relative expression of each protein was quantified using ImageJ analysis software.

2.5. HUVECs morphology and collagen expression

HUVECs were fixed with glutaraldehyde and dehydrated through graded ethanol solutions (30%, 50%, 70%, 90% and 100%) and critical point drying following 3-day incubation on the scaffolds. The morphology of HUVECs was observed using environmental scanning electron microscope (Quanta 200 FEG).

HUVECs of 2×10^4 were seeded on PLA@Gel/CF3 or PLA@Gel in 24-well culture plates. After 2-day culture, trypsin/EDTA (Ethylene Diamine Tetraacetic Acid) was added and cells were removed. The scaffolds left were washed, blocked with 1% BSA(bovine serum albumin)/PBS, and incubated with rabbit anti-human type IV collagen (GeneTex) for 1 h. The HRP (horseradish peroxidase)-conjugated goat anti-rabbit IgG (Abcam) was added, followed by TMB (Tetramethyl benzidine) substrate addition. The absorbance at 450 nm was measured with a microplate reader (BioTek).

2.6. HUVEC migration and angiogenesis with NRCMs conditioned medium

NRCMs (1×10^6) were seeded on PLA@Gel or PLA@Gel/CF3 in a 6-well culture plate. After 48 h-incubation, the medium without 5-BrdU were added and the cells were cultured for another 48 h, the supernatants were collected as conditioned medium (CM).

HUVECs (2×10^5 cells) were cultured in 24-well plate and a straight line was scratched across with a 200 μL pipet tip when the cells became confluent. Thereafter, CM of 500 μL was added to HUVECs. The cells were observed under microscope (Olympus IX71) at 0 h, 6 h, 12 h, and 24 h. The wound width was analyzed with ImageJ software.

HUVECs (3×10^4 cells) were seeded in the growth factor reduced Matrigel (BD) in 96-well culture plate. The CM of 100 μL was added into the wells and incubated for 12 h with supplemented calcein-AM (Molecular Probe). The tube number and total tube length were quantified by ImageJ analysis software in five randomly selected fields at 4 × magnification.

2.7. Left ventricular ligation and cardiac patch implantation

Adult SD male rats were randomly divided into four groups (8 rats per group). After being anesthetized with isoflurane, the rats were intubated and connected to the ventilator (Kent Scientific). The rats' hearts were exposed, and the left anterior descending coronary artery (LAD) was ligated with a 7-0# needle suture. The electrocardiograph (ECG) displayed a T wave inversion (II lead) after the ligation, indicating the myocardial infarction (M.I.) model successful establishment. Patches of PLA@Gel or PLA@Gel/CF3 of 6 mm in diameter were carefully placed to the M.I. area and manual compression was applied. For the control group, the chest of rats was closed after the ligation. For the sham group, the animals were operated with the same procedure without ligation.

2.8. Transthoracic conventional echocardiography

Standard parasternal long-axis ultrasound examination was performed using a 13–24 MHz linear-array transducer (MS-250) with a digital Vevo 2100 small animal ultrasound system (FUJIFILM VisualSonics Inc., Toronto, Canada). The Rats were anesthetized with 2% isoflurane and were placed on thermostatic platform. B- and M-mode scans were applied at the midventricular level and cine loop images (300 frames) were stored. Speckle-tracking echocardiography (STE) was performed in the PSLAX view at the B-Mode cine loops to provide the reproducible orbits of myocardial movements. Measurements were obtained from four consecutive cardiac cycles by using the VevoLab software (Version 5.6.0, FUJIFILM). The movement at each point was displayed as blue when the tissue was moving away from the apex and as red when the tissue was moving towards the apex. The following cardiac functions parameters were collected, LV ejection fraction (EF %), LV fractional shortening (FS %), LV cardiac output (ml/min) and global longitudinal strain (GLS). The negative GLS values indicated cardiac fiber shortening. At the end of the examination, all rats recovered from aesthesia.

2.9. Histochemical assay

On day-27 after the implantation, the rats were sacrificed, the heart were separated and collected. After being injected with 4% paraformaldehyde through the aorta to remove the blood, the hearts were immediately immersed in the paraformaldehyde solution (4% in PBS) overnight. After conventional processing, paraffin-embedded sections were stained with hematoxylin/eosin (H&E), Masson trichrome and primary antibodies of rabbit anti-Cx43 and anti-α-SMA (1:500). After washing, the immunohistology sections were further stained with corresponding fluorescence second antibody and DAPI.

2.10. Statistical analysis

All experiments were performed at least three times. Three replications were set for each experiment at least. For cell experiments, Data were presented as means ± SD. For animal experiment, data were presented as means ± SEM. Multiple comparisons of different groups were analyzed using GraphPad Prism Software (V.5) with one-way ANOVA. Two groups comparisons were analyzed using *t*-test. The p values lower than 0.05 were considered statistically significant, $^*p < 0.05$, $^{**}p < 0.01$.

3. Results

3.1. Preparation and characterization of composite scaffolds

SEM images showed that the electrospun fibers were homogenous (Fig. 1A) with the average diameter of 760 nm (Fig. 1B). With the addition of gold nanoparticles in the PLA solution in the electrospinning, the core-shell structure was clearly seen (inserted figure) due to the higher density of the gold nanoparticles. The nanofibrous film could be cut into small pieces and dispersed in tert-butanol by homogenizing (Fig. S1A), and the majority of the length for CFs dispersed in tert-butanol was not longer than 1 mm (Fig. S1B). In the composites, it could be seen that the CFs was distributed in the porous composite scaffolds (Fig. 1C). Moreover, the resulting scaffolds were easy to mold into designed shapes (Fig. 1D).

The incorporation of CFs improved the physical properties of the scaffolds. As shown in Fig. 2A, the density of the scaffolds decreased with the increase of CFs content, suggesting the scaffolds with more CFs obtained larger porous volume compared with the control scaffold with the same mass. This is likely because CFs provided rigid support for the porous structure of the scaffolds, which resisted the volume shrinkage in the cross-linking and lyophilization process. At the same time, as the porous volume increased, the water absorption capacity for the scaffolds was increased as well (Fig. 2B), the maximum water absorption of PLA@Gel, PLA@Gel/CF1, PLA@Gel/CF3, and PLA@Gel/CF5 at 5 min was 964.33%, 1025.99%, 1142.28% and 1206.93% respectively, indicating that the composite scaffolds were able to hold more aqueous solution. The porosity of the scaffolds was increased proportionally with the addition of CFs (Fig. 2C). After adsorbing water, the scaffold became dark and was easily to be folded (Fig. 2D, Video S1). Interestingly, the compressive stress-strain of the scaffolds was significantly improved along with the increase of CFs content (Fig. 2E). Considering the compression strain-stress curves were measured with the dry scaffolds and the scaffolds would inevitably contact water in the application, the curves of water swelled PLA@Gel and PLA@Gel/CF3 were measured as

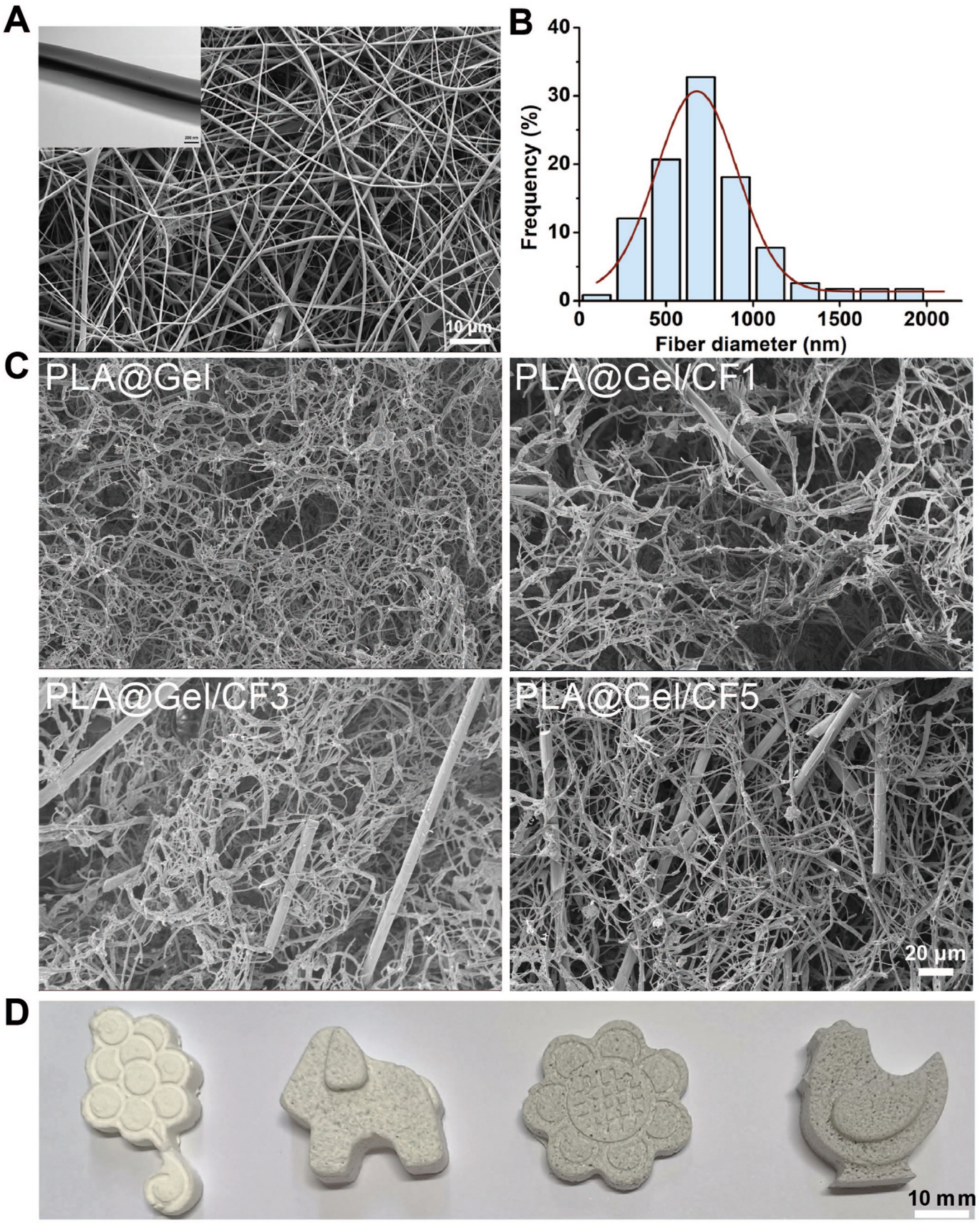

Fig. 1. Morphology of the fibrous film and the composite scaffolds. (A) Images of SEM and TEM (inserted) for the co-axial electrospun fibers. (B) Diameter distribution of the electrospun fibers. (C) SEM images of the composite scaffold PLA@Gel, PLA@Gel/CF1, PLA@Gel/CF3 and PLA@Gel/CF5. (D) Photographs of the cartoon composite scaffolds made of PLA@Gel, PLA@Gel/CF1, PLA@Gel/CF3, and PLA@Gel/CF5 (from left to right) with different shapes.

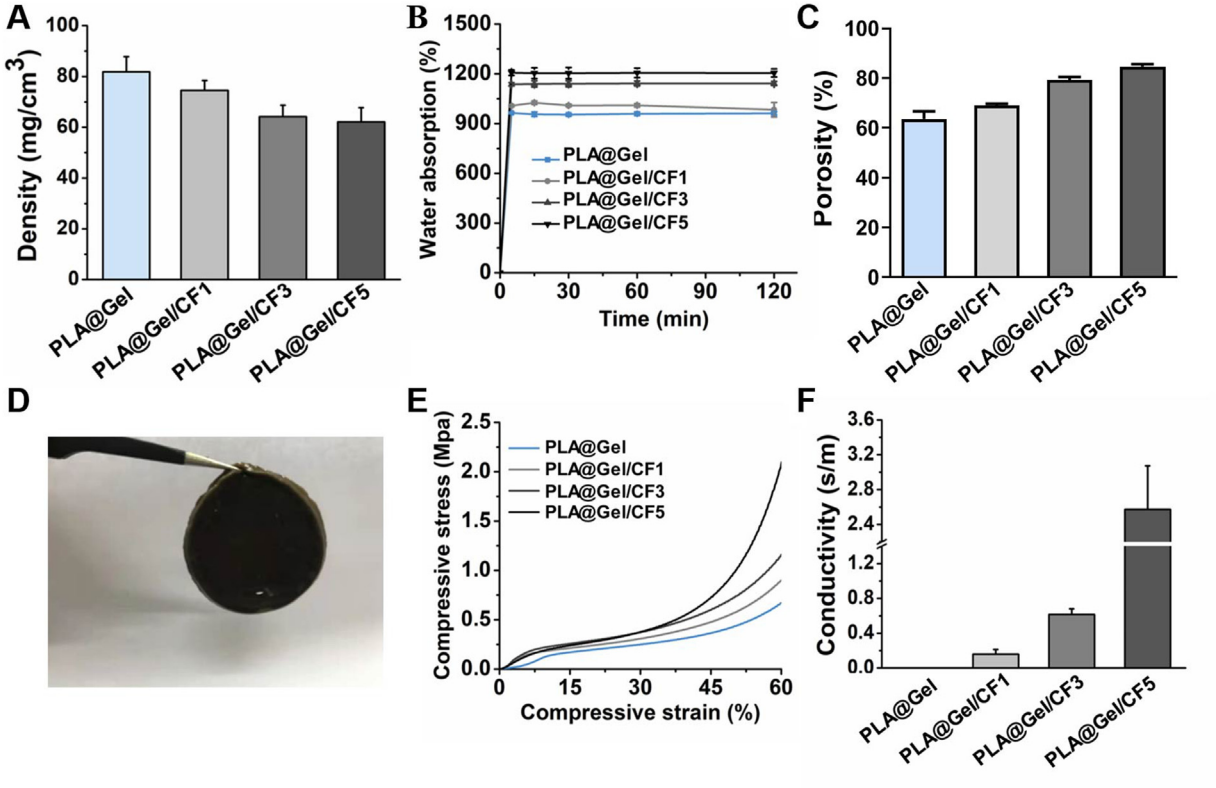

Fig. 2. Physical properties of the composite scaffolds. (A) Density (n = 3), (B) water absorption percentage (n = 3), (C) Porosity (n = 3), (D) photograph of conductive composite scaffold of PLA@Gel/CF3 after soaking in water, (D) compressive stress-strain curves, and (E) conductivity of the scaffolds (n = 3).

well, and the elastic moduli of the swelled scaffolds were 145.3 kPa and 389.7 kPa respectively (Fig. S2), which were located in the range of that for natural rat heart during diastole and systole [32]. Besides, the conductivity of PLA@Gel/CFs was significantly increased compared with that of PLA@Gel (Fig. 2F), which was attributable to the excellent conductivity of CFs [33,34]. Importantly, the electrical conductivity of PLA@Gel/CF1 and PLA@Gel/CF3 was 0.16 S/m and 0.58 S/m, respectively, which fell in the conductivity range of ventricular muscle, blood, and skeletal muscle (0.03–0.6 S/m) [35]. Considering that in the suitable conductivity range, higher conductivity would harness and facilitate cardiomyocytes viability [36], and it would be better for scaffolds to have lower density and higher swelling ratio, in the following experiments, PLA@Gel/CF3 was selected as a representative of the conductive composite scaffold, and PLA@Gel was used as control.

3.2. PLA@Gelatin/CF3 enhanced NRCMs maturation

The neonatal rat cardiomyocytes (NRCMs) proliferated at a similar rate on PLA@Gel/CF3 and PLA@Gel according to the results of the cell viability (Fig. 3A). Physiological functions of the cells grown on the two scaffolds were evaluated by examining the expression of connexin-43 (Cx43), cardiac α-sarcomeric actinin (α-actinin) and RhoA, because Cx43 forms gap junction channel to accomplish intercellular electrical coupling and regulates electrical signal transmission between NRCMs [35,37], α-actinin is a cardiac-specific contractile protein for myofilament reassembly [38], and Rho family small GTPases like RhoA is reported to regulate cell-cell junctions [39,40]. The results showed that NRCMs grown on PLA@Gel/CF3 expressed significantly higher level of Cx43, α-actinin and RhoA compared with those on PLA@Gel (Fig. 3B and C), indicating the addition of CFs enhanced the intercellular adhesive junctions and electrochemical junctions in the NRCMs. It could be noted that the level of HIF-1α for NRCMs grown on PLA@Gel/CF3 was significantly up-regulated compared with those on PLA@Gel (Fig. 3B and C). As HIF-1α plays a central role in regulating VEGF [41], and VEGF is one of the most important growth factors regulating neovascularization, the production of VEGF for the cells was measured, showing that NRCMs grown on PLA@Gel/CF3 produced more VEGF than the control (Fig. 3D), indicating that the conductive composite scaffolds could enhance the cells to establish an angiogenic microenvironment that was beneficial for recruiting endothelial cells to realize neovascularization.

3.3. PLA@Gel/CF promoted HUVECs angiogenesis

Next, we investigated whether the scaffolds could support the growth of vascular endothelial cells and induce vascularization. Both PLA@Gel and PLA@Gel/CF3 were able to well support the growth of HUVECs (Fig. 4A). Moreover, western blot results showed that the level of VE-cadherin, Cx43, CD31, and RhoA was all up-regulated significantly for HUVECs grown on PLA@Gel/CF3 compared with that for the cells grown on PLA@Gel (Fig. 4B and C). VE-cadherin is particularly important in neovascularization [42], Cx43 forms the gap junction channel that regulates electrical signal transmission between cells, CD31 makes up the intercellular junctions between endothelial cells [43], and RhoA plays a key role in regulating angiogenesis [44]. These results indicated that the conductive composite scaffolds could provide angiogenesis stimulus for HUVECs. Noted that HUVECs grown on PLA@Gel/CF3 were able to form vessel-like structures and exhibit a spreading morphology, on the contrary, HUVECs grown on PLA@Gel mainly displayed separate and flat appearance (Fig. 4D). These results suggested that the conductive CFs facilitate the endothelial cell vessel-like structure formation, which is an important indicator of angiogenesis. We further investigated whether HUVECs grown on PLA@Gel/CF3 maintained the anticoagulant function. The results showed that HUVECs grown on PLA@Gel/CF3 secreted less PAI-1, indicating the conductive scaffold was favor for maintaining the anticoagulant function than those on PLA@Gel (Fig. 4E). In addition, HUVECs grown on PLA@Gel/CF3 produced much more Type IV collagen

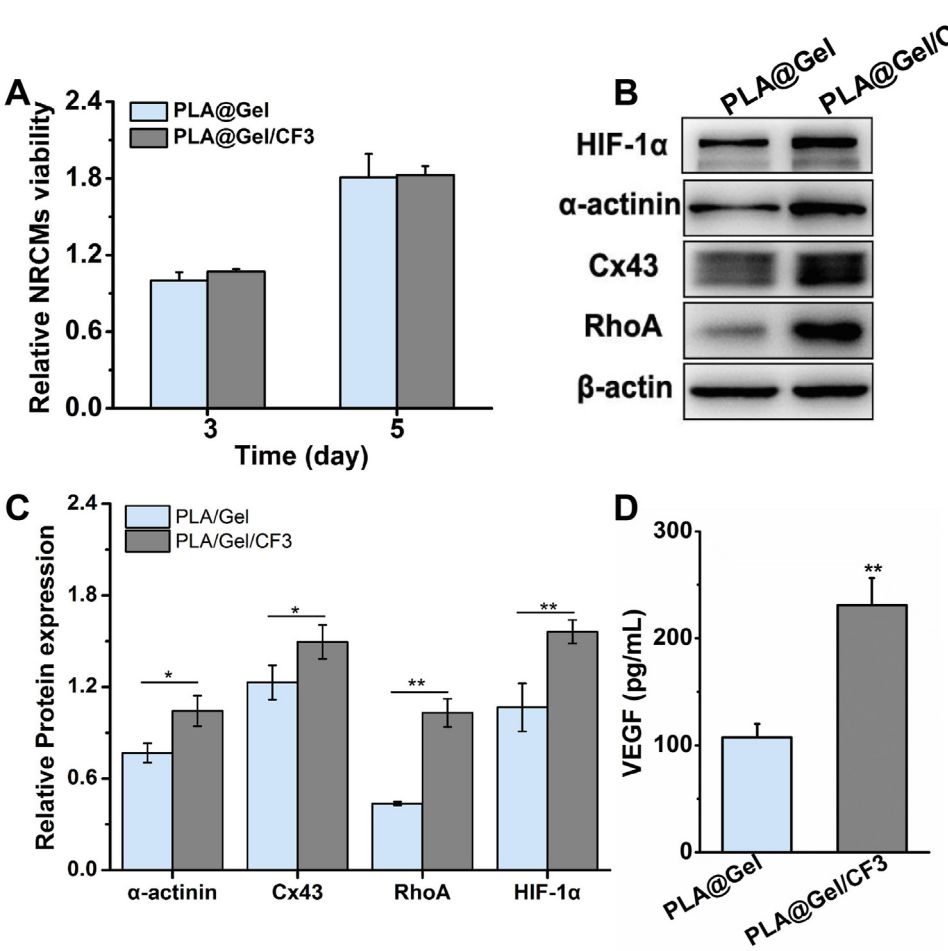

Fig. 3. PLA@Gel/CF3 enhanced NRCMs maturation and recruited endothelial cells. (A) Cell viability of NRCMs grown on the scaffolds for 3 or 5 days (n=4). (B) Representative bands of western blot for HIF-1α, α-actinin, Cx43, and RhoA for NRCMs. (C) Quantification expression of HIF-1α, α-actinin, Cx43, and RhoA for NRCMs (n=3). (D) VEGF secreted by NRCMs (n=3). *p < 0.05, **p < 0.01 vs that of PLA@Gel.

(Fig. 4F) that can initiate angiogenetic response and result in the formation of a new basement membrane [45].

3.4. PLA@Gel/CF3 enhanced the crosstalk between cardiomyocytes and endothelial cells

The supernatants of NRCMs grown on PLA@Gel and PLA@Gel/CF3 were supplemented in the culture system of HUVECs, referred as CM/PLA@Gel and CM/PLA@Gel/CF3 respectively. The HUVECs treated with CM/PLA@Gel/CF3 showed a quick gap close (Fig. 5A), indicating that the CM promoted the endothelial cells proliferation and migration. Meanwhile, the cells formed more vessel-like tubes than those incubated with CM/PLA@Gel (Fig. 5B). The average tube number and tube length was increased to 1.8 folds and 1.2 folds respectively for the HUVECs incubated with CM/PLA@Gel/CF3 compared to that with CM/PLA@Gel (Fig. 5C and D). These results indicated that the NRCM grown on PLA@Gel/CF3 could sense the physical characteristics and transfer them in the form of biochemical cues, enhancing the endothelial cells functions by the effective crosstalk between the two types of the cells.

3.5. Echocardiographic analysis of rat cardiac function

The synchronized contraction of M.I. heart with/without the implantation of the scaffolds was recorded by the echocardiography (Videos S2–4, supporting information) 3 weeks post the scaffolds implantation. It could be seen that the local muscle movements of the infracted area were different, though the hearts continued to contract and dilatate in all the groups. First, from the images of M-Mode (Fig. 6A), it could be seen that the LV anterior wall (LVAW, red arrow) ultrasonic scattering density was very low for the M.I. group, indicating the heart muscles were damaged. The scaffolds implantation increased the LVAW ultrasonic scattering density, especially PLA@Gel/CF3. To clarify the detail of LVAW movements, speckle tracking analysis was applied (see B-Mode in Fig. 6A). The strain-based orbit line mapping showed that the muscle movements of the M.I. heart was limited with a shorten orbit (yellow arrow), implying the strength of muscle was decreased. The muscles function was recovered with increased orbit of muscle movement (blue arrow), demonstrating that the PLA@Gel/CF3 implantation retarding the injury. The 3D global left ventricle radial and longitudinal strain displayed a discordant color of the muscle movement, indicating the infracted area was passive to the whole heart movement. PLA@Gel/CF3 improved the coordination of the infracted muscle, providing another proof that the composite scaffolds were benefit for infracted muscle regeneration. These results indicated that the contraction and dilation of the cardiac function were improved by PLA@Gel/CF3 implantation.

The movement difference for the infracted area could be reflected by the cardiac function indicators calculated from the echocardiography analysis, including LV ejection fractions (EF, %), fractional shortening (FS, %), cardiac output (CO) and global longitudinal strain (GLS) (Fig. 6B). Rats of M.I. group displayed decrease of EF, FS and CO. The implantation of scaffolds increased the EF, FS, and CO of LV. In particular, the GLS was significantly enhanced by PLA@Gel/CF3. These results together proved that the cardiac dysfunction induced by myocardia infraction was reversed by the PLA@Gel/CF3 implantation.

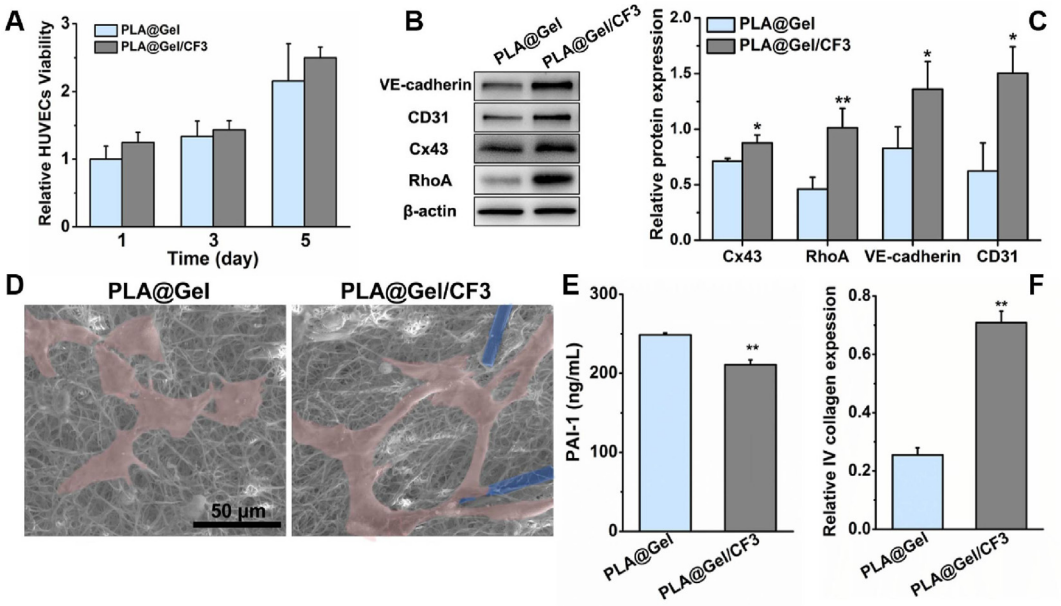

Fig. 4. Morphology and functions of HUVECs grown on the composite scaffolds. (A) Cell viability of different incubation time determined by CCK-8 assay (n=4). (B) Representative western blot bands showing the expression of VE-cadherin, CD31, Cx43 and RhoA. (C) Quantification of the western blot results (n=3). (D) ESEM images of HUVECs (pink) and carbon fibers (blue) in the scaffolds. The level of plasminogen activator inhibitor-1 (PAI-1) (E) and type IV collagen (F) secreted by HUVECs grown on the scaffolds for 2 days. (n=3). *p < 0.05, **p < 0.01 vs that of PLA@Gel.

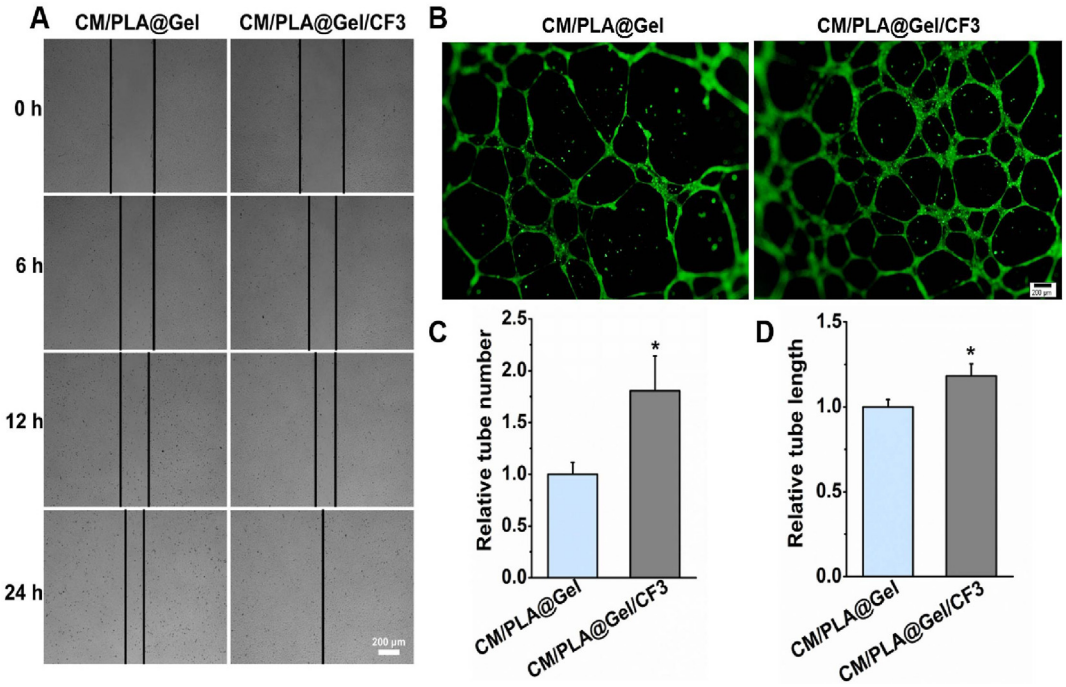

Fig. 5. Conductive composite scaffolds enhanced the crosstalk between NRCMs and HUVECs. (A) Wound healing of HUVECs at different times. The supplement of CM/PLA@Gel/CF3 increased the HUVECs migration and proliferation with a quick gap close. (B) Representative endothelia cell tube formation in conditioned media. Quantification of the tube number (C) and length (D) for HUVECs in conditioned media, n=5. *p < 0.05 vs that of PLA@Gel.

3.6. Histological analyses of rat cardiac structure

Hematoxylin/eosin (H&E) and Masson staining (Fig. 7A) showed the infracted heart wall of the M.I. rats became thin and was filled with scar tissues, composed of collagen and fibroblast cells, and muscle cells were hardly seen in the scar tissues. The pathology characteristics were consistent with the speckle tracking analysis of the decreased longitudinal strain because of the infraction. The PLA@Gel scaffold implantation was able to inhibit the infracted heart wall to become thin, and the heart wall was composed of loose collagen fibers, fibroblast cells and scattered heart muscle cells, indicating that the muscles injury was attenuated. For the group of PLA@Gel/CF3 implantation, the infracted heart wall showed the most thickness in the three groups, at the same time, the scar area was the smallest; only a small part of the heart tissue was stained blue, implying that most of the area was filled with cardiomyocytes instead of scar tissue. The thickness of the heart wall and relative area of the heart muscle in the infracted area were calculated from five random fields of each group with 20 × magnification. The results showed that the

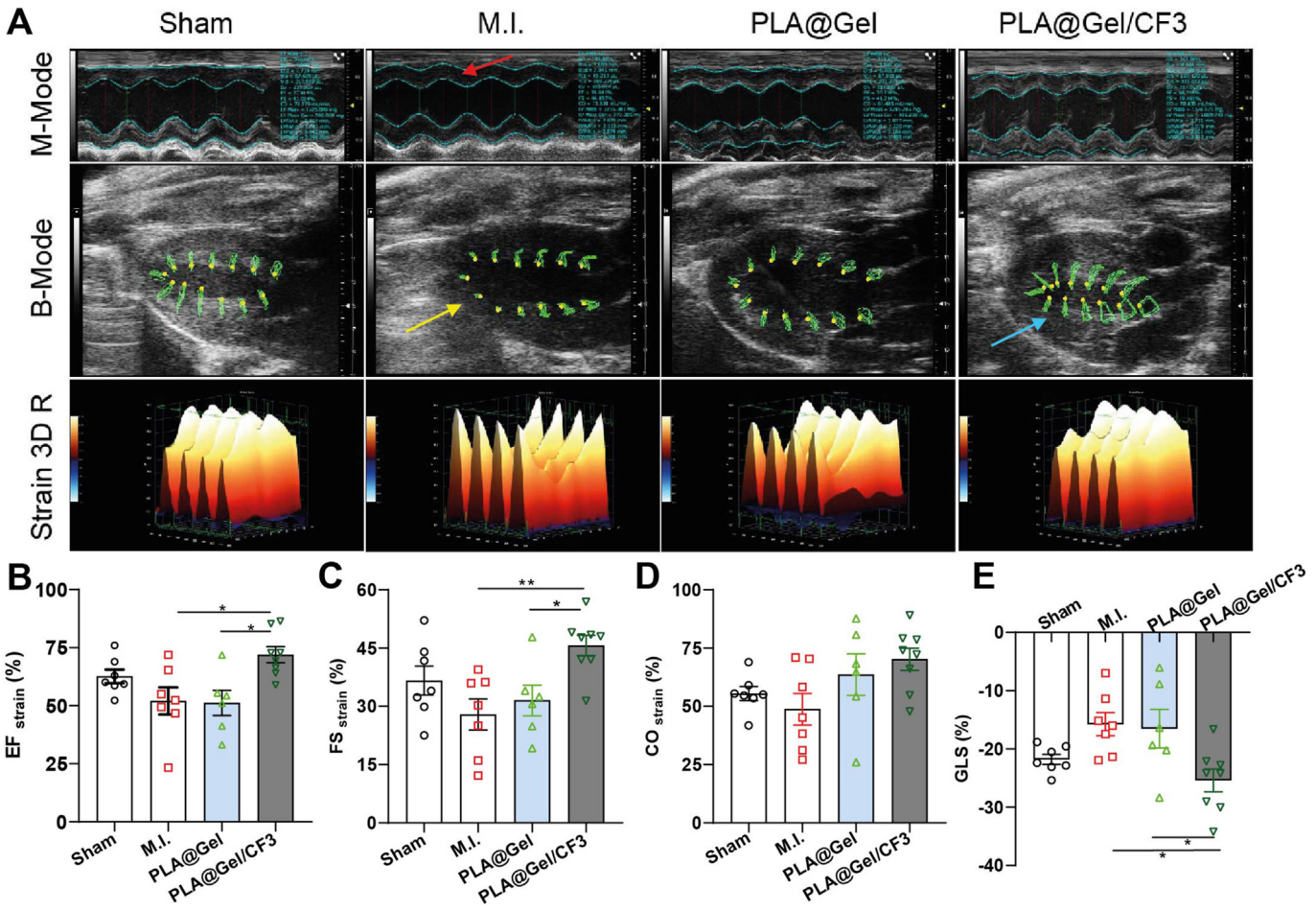

Fig. 6. Effects of the implanted scaffolds on the LV function and movement. (A) Representative M-Mode, B-Mode, and 3D global left ventricle longitudinal strain movement images for different groups. PLA@Gel/CF3 implantation improved the LV movement coordination. Differences of hearts EF (B), FS (C), CO (D), and GLS (E) for the rats of the four groups. For sham and M.I. groups, n=7; for PLA@Gel group, n=6; for PLA@Gel/CF3 group, n=8; *p < 0.05, **p < 0.01.

heart wall was thicker with the implantation of PLA@Gel/CF3 than that of PLA@Gel as well as that of the M.I. groups, and the thickness was similar to that of the healthy rats (Fig. 7B). At the same time, the heart muscle area was significantly increased for the PLA@Gel/CF3 group compared with that of PLA@Gel group, meanwhile, the collagen area was decreased (Fig. 7C).

The immunohistological staining of Cx43 and α-SMA was applied to the heart tissue (Fig. 8A), showing that there were no Cx43 positive cells observed in the tissue of the infracted area for M.I. group, demonstrating the muscle tissue were totally replaced by the scar. For PLA@Gel implantation group, the Cx43 expression was increased to a certain extent in reference to the M.I. group though the level was still low. For the PLA@Gel/CF3 group, the expression of Cx43 was significantly increased, strongly suggested effective tissue regeneration in the infraction area. In addition, α-SMA staining indicating blood vessel structure was examined. Among the three groups, more blood vessels stained with circular α-SMA positive structure could be seen in the PLA@Gel/CF3 group. By comparison, one could see many vessel structures with very small diameters in the heart with implantation of PLA@Gel, while more vessel structures with larger diameters were observed in the heart with PLA@Gel/CF3 suggesting that the implantation of PLA@Gel/CF3 promoted angiogenesis that beneficial to the myocardial regeneration. The angiogenesis of the tissue was evaluated with the vessel density indicated by the α-SMA positive circular structures. The statistical analysis was performed by counting the circular structure five random fields of each group under 40 × magnification. The results showed that the PLA@Gel/CF3 scaffolds significantly increased the vessel density, which was about 3 times of that of M.I, and significantly higher than that of PLA@Gel as well (Fig. 8B).

4. Discussion

Scaffolds stand the central position in guiding tissue regeneration. For uses in cardiac tissue engineering, scaffolds need sufficient stiffness and conductivity as well as fibrous structures that provide environment mimicking the heart muscle. Although electrospinning technique has been widely applied to generate fibrous scaffolds in the cardiac tissue regeneration [20,46], it was usually applied to produce fibrous membranes instead of three-dimensional scaffolds. In addition, the stiffness of fibrous membranes alone usually is too low to meet the requirement of cardiac tissue contraction. Besides stiffness, it has been recognized that conductivity is necessary and holds certain advantages in aspect of enhancing cardiomyocyte maturation and electrophysiological function [19]. Up to date, various conductive nanomaterials have been explored to increase the conductivity of insulating polymeric materials effectively, mainly including carbon nanotubes [21,47,48], graphene [19,49], and gold nanoparticles [22,50].

One advantage of the present study is the utilization of carbon fibers (CFs). CFs have high strength and high modulus, therefore can be an ideal reinforcing material [51,52]. Additionally, CFs hold attractive electrical conductivity that is even close to that of metals [33,34]. Different from

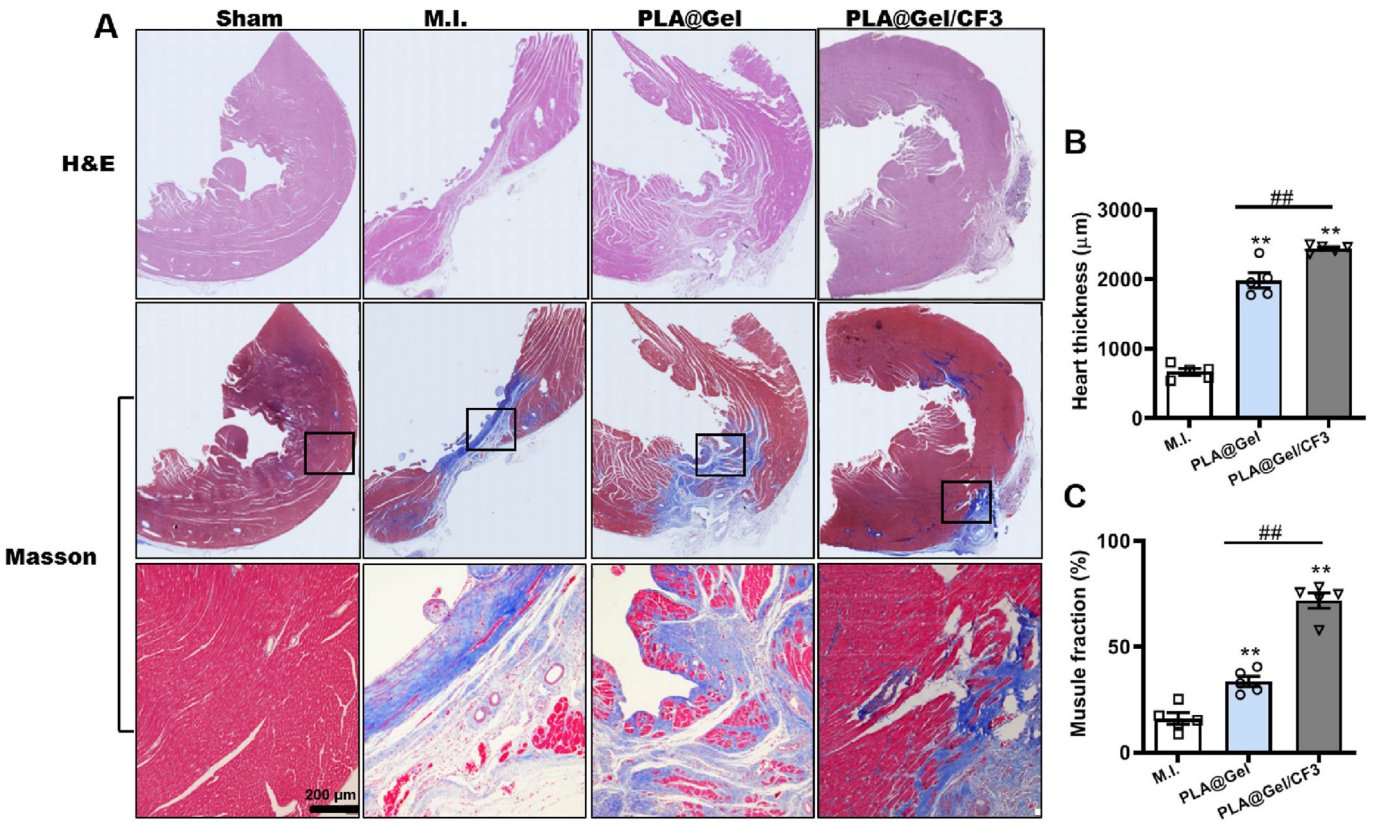

Fig. 7. Histochemical observations of M.I. heart of rats with scaffolds implantation. A. Hematoxylin/eosin (H&E, first row) and Masson's trichrome staining (second and third row) of the infracted heart wall post 4 weeks of the implantation. Collagen was stained in blue and muscle in red. Heart wall thickness (B) and muscle area (C) of the infracted heart for the M.I., PLA@Gel, and PLA@Gel/CF3 group (n = 5), **p < 0.01 vs that of M.I., ##<0.05.

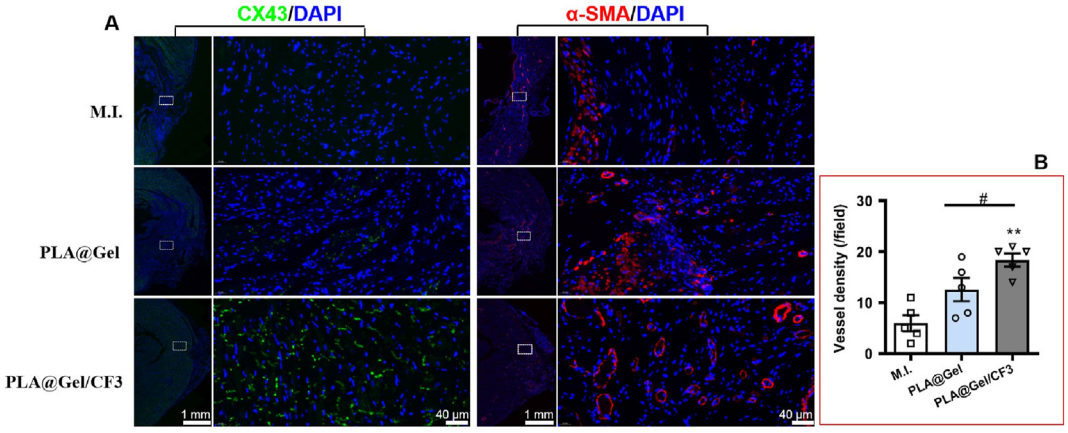

Fig. 8. Immunofluorescence of muscle and vessel maturation for the infracted heart of rat received different treatments post M.I. A. Representative image of Cx43 (green) and α-SMA (red), the nuclear was co-stained with DAPI (blue). B. The calculation of vessels density in the infracted heart for different groups (n = 5), **p < 0.01 vs that of M.I., #<0.05.

conductive nanomaterials in size, CFs are a kind of conductive fibers with a diameter of 7 μm that is close to the size of purkinje fiber transducing electrical signals in myocardial tissue. In this work, CFs were applied to act not only as a rigid supportive frame for the soft fibrous matrix, but also as conductive fibers mimicking micro-scaled purkinje fibers in the heart. Additionally, as one kind of carbon materials, CFs provided the compatibility to the cardiomyocytes and vascular endothelial cells, which will be further discussed below.

In the development of conductive 3D scaffolds, it would be better to fabricate the scaffolds by more flexible ways. In this work, the techniques of co-axial electrospinning and freeze-drying were combined to fabricate the 3D composite scaffolds, which could mold the scaffold into various shapes easily as well as integrating the advantages of hydrogel and nanofibrous scaffold. In the composition of the coaxial fibers, PLA was selected as the core content, because the hydrophobicity of PLA hinders the adhesion and proliferation of cells [53] while its tensile strength is necessary for the fibers, and gelatin was used as the shell, because it contains lysine and arginine residues with positive charge and specific cell adhesion site, which has better biocompatibility and can promote cell adhesion [54,55]. At the same time, CFs provided the mechanical support to allow the formation of 3D scaffolds. By this simple approach, the porosity and modulus of the prepared scaffolds were comparable with the

electroactive 3D scaffold composed of silk fibroin and conducting poly(anilineco-N-(4-sulfophenyl) aniline) (PASA), while the conductivity was higher [56].

It was noticeable that the expression of HIF-1α for NRCMs grown on PLA@Gel/CF3 was significantly increased, which was attributable to the hypoxia caused by the stronger beating of NRCMs grown on the scaffold that had higher stiffness than control [34]. It has been well documented that HIF-1α can mediate the expression of VEGF gene and promote angiogenesis during tissue repair under hypoxia [41]. In the present study, it was found out that NRCMs on PLA@Gel/CF3 expressed a higher level of VEGF than those on PLA@Gel. Therefore, we would suggest that PLA@Gel/CF3 is capable of enhancing NRCMs to secrete VEGF by inducing a proper hypoxic status of the cells, which recruited and promoted the endothelial cells to form vessel-like structures.

Rapid formation of confluent endothelial layer is critical for vascular remodeling and myocardial tissue engineering. Here we tried to figure out whether the NRCMs could transfer the cues of scaffolds to the HUVECs, which would be beneficial to the recruitment of endothelial cells into the scaffolds. It was interesting that the NRCMs could sense the different features of the scaffolds and deliver the beneficial environmental cues to the HUVECs by secreting more VEGF that directly participates in angiogenesis by recruiting endothelial cells to hypoxic and avascular areas and by stimulating their proliferation, which led to the more vessel-like structures formation (Fig. 4D). On the other hand, the conductive 3D composite scaffold of PLA@Gel/CF3 could interact with HUVECs directly as well. It has been documented that carbon materials can have various protein molecules strongly adsorbed on their surface, which makes the surface blood compatible [57–59]. Therefore, the integration of CFs would provide more friendly interface to the endothelial cells. Additionally, it has been recognized that utilizing electroactive materials in scaffolds can greatly improve the functional outcomes of cells [60]. Although endothelial cells are not inherently electrically dependent, the conductive composite noticeably increased the cells proliferation and NO release [43]. It should be noted that the level of Cx43 and VE-cadherin was up regulated significantly when HUVECs were grown on PLA@Gel/CF3, indicating the conjugation for the cells was enhanced, and that is essential for endothelial cells to maintain cell-cell communication, which subsequently directs endothelial cell morphogenesis and guides the development and integrity of confluent endothelial monolayer [55]. Meanwhile, RhoA was also increased. The higher expression of RhoA would benefit the organization of cytoskeleton and cell morphology and enhanced the migration and angiogenesis of HUVECs in vitro [61]. Taken above together, the scaffold PLA@Gel/CF3 was able to enhance the growth of endothelial cells and the formation of vessel-like structures through cell-cell interaction and cell-scaffold interaction.

5. Conclusion

A novel 3D conductive composite scaffold was fabricated by integrating carbon fibers and co-axial fibers, which possessed proper conductivity, stiffness and fibrous structures. The conductive composite scaffold not only enhanced NRCMs maturation and VEGF production, but also promoted HUVECs to form vessel-like structures and to keep the anticoagulant function, moreover, enhanced the crosstalk between the NRCMs and HUVECs. These effects together led to the functional heart tissue regeneration post myocardial infarction.

CRediT author statement

Jie Meng: Investigation, Methodology, Validation, Writing – original draft, Formal analysis. Bo Xiao: Investigation, Validation. Fengxin Wu: Investigation, Writing – original draft. Lihong Sun: Validation, Formal analysis. Bo Li, Wen Guo, Xuechun Hu, Xuegai Xu, Tao Wen: Investigation. Jian Liu: Writing – review & editing, Funding acquisition. Haiyan Xu: Conceptualization, Methodology, Writing-Reviewing and Editing, Supervision, Funding acquisition.

Authors' contributions

The manuscript was written through contributions of all authors. All authors have given approval to the final version of the manuscript. # These authors contributed equally to this work.

Declaration of competing interest

The authors declare that they have no known competing financial interests or personal relationships that could have appeared to influence the work reported in this paper.

Acknowledgements

This work was supported by National Key R&D program of China (2017YFA0205504), National Natural Science Foundation of China (NSFC 81971366). and CAMS Innovation Fund for Medical Sciences (CIFMS) (2021-I2M-1–006).

Appendix A. Supplementary data

Supplementary data to this article can be found online at https://doi.org/10.1016/j.mtbio.2022.100415.

References

[1] G.R. Ferrier, I.M. Redondo, C.A. Mason, C. Mapplebeck, S.E. Howlett, Regulation of contraction and relaxation by membrane potential in cardiac ventricular myocytes, Am. J. Physiol. Heart Circ. Physiol. 278 (5) (2000 May) H1618–H1626.
[2] K.L. Fujimoto, K. Tobita, W.D. Merryman, J. Guan, N. Momoi, D.B. Stolz, M.S. Sacks, B.B. Keller, W.R. Wagner, An elastic, biodegradable cardiac patch induces contractile smooth muscle and improves cardiac remodeling and function in subacute myocardial infarction, J. Am. Coll. Cardiol. 49 (23) (2007 Jun 12) 2292–2300.
[3] S. He, H. Song, J. Wu, S.H. Li, R.D. Weisel, H.W. Sung, J. Li, R.K. Li, Preservation of conductive propagation after surgical repair of cardiac defects with a bio-engineered conductive patch, J. Heart Lung Transplant. 37 (7) (2018 Jul) 912–924.
[4] Y. Zhu, Y. Matsumura, W.R. Wagner, Ventricular wall biomaterial injection therapy after myocardial infarction: advances in material design, mechanistic insight and early clinical experiences, Biomaterials 129 (2017 Jun) 37–53.
[5] E. Tzahor, K.D. Poss, Cardiac regeneration strategies: staying young at heart, Science 356 (6342) (2017 Jun 9) 1035–1039.
[6] A. Uygur, R.T. Lee, Mechanisms of cardiac regeneration, Dev. Cell 36 (4) (2016 Feb 22) 362–374.
[7] W. Chen, S. Chen, Y. Morsi, H. El-Hamshary, M. El-Newhy, C. Fan, X. Mo, Superabsorbent 3D scaffold based on electrospun nanofibers for cartilage tissue engineering, ACS Appl. Mater. Interfaces 8 (37) (2016 Sep 21) 24415–24425.
[8] W. Chen, J. Ma, L. Zhu, Y. Morsi, , -Ei-Hamshary H, S.S. Al-Deyab, X. Mo, Superelastic, superabsorbent and 3D nanofiber-assembled scaffold for tissue engineering, Colloids Surf. B Biointerfaces 142 (2016 Jun 1) 165–172.
[9] X. Mei, K. Cheng, Recent development in therapeutic cardiac patches, Front. Cardiovasc. Med. 7 (2020 Nov 27), 610364.
[10] R. Dong, P.X. Ma, B. Guo, Conductive biomaterials for muscle tissue engineering, Biomaterials 229 (2020 Jan), 119584.
[11] S. Liang, Y. Zhang, H. Wang, Z. Xu, J. Chen, R. Bao, B. Tan, Y. Cui, G. Fan, W. Wang, W. Wang, W. Liu, Paintable and rapidly bondable conductive hydrogels as therapeutic cardiac patches, Adv. Mater. 30 (23) (2018 Jun), e1704235.
[12] B.W. Walker, R.P. Lara, C.H. Yu, E.S. Sani, W. Kimball, S. Joyce, N. Annabi, Engineering a naturally-derived adhesive and conductive cardiopatch, Biomaterials 207 (2019 Jul) 89–101.
[13] A. Mihic, Z. Cui, J. Wu, G. Vlacic, Y. Miyagi, S.H. Li, S. Lu, H.W. Sung, R.D. Weisel, R.K. Li, A conductive polymer hydrogel supports cell electrical signaling and improves cardiac function after implantation into myocardial infarct, Circulation 132 (8) (2015 Aug 25) 772–784.
[14] M. Kapnisi, C. Mansfield, C. Marijon, A.G. Guex, F. Perbellini, I. Bardi, E.J. Humphrey, J.L. Puetzer, D. Mawad, D.C. Koutsogeorgis, D.J. Stuckey, C.M. Terracciano, S.E. Harding, M.M. Stevens, Auxetic cardiac patches with tunable mechanical and conductive properties toward treating myocardial infarction, Adv. Funct. Mater. 28 (21) (2018), 1800618.
[15] Y. Wu, L. Guo, Enhancement of intercellular electrical synchronization by conductive materials in cardiac tissue engineering, IEEE Trans. Biomed. Eng. 65 (2) (2018) 264–272.

[16] Y. He, G. Ye, C. Song, C. Li, W. Xiong, L. Yu, X. Qiu, L. Wang, Mussel-inspired conductive nanofibrous membranes repair myocardial infarction by enhancing cardiac function and revascularization, Theranostics 8 (18) (2018 Oct 6) 5159–5177.
[17] S.R. Shin, C. Zihlmann, M. Akbari, P. Assawes, L. Cheung, K. Zhang, V. Manoharan, Y.S. Zhang, M. Yuksekkaya, K.T. Wan, M. Nikkhah, M.R. Dokmeci, X.S. Tang, A. Khademhosseini, Reduced graphene oxide-GelMA hybrid hydrogels as scaffolds for cardiac tissue engineering, Small 12 (27) (2016) 3677–3689.
[18] G. Zhao, X. Zhang, T. Lu, F. Xu, Recent advances in electrospun nanofibrous scaffolds for cardiac tissue engineering, Adv. Funct. Mater. 25 (36) (2015) 5726–5738.
[19] L. Wang, Y. Wu, T. Hu, B. Guo, P.X. Ma, Electrospun conductive nanofibrous scaffolds for engineering cardiac tissue and 3D bioactuators, Acta Biomater. 59 (2017) 68–81.
[20] Y. Wu, L. Wang, B. Guo, P.X. Ma, Interwoven aligned conductive nanofiber yarn/hydrogel composite scaffolds for engineered 3D cardiac anisotropy, ACS Nano 11 (6) (2017) 5646–5659.
[21] J. Ren, Q. Xu, X. Chen, W. Li, K. Guo, Y. Zhao, Q. Wang, Z. Zhang, H. Peng, Y.G. Li, Superaligned carbon nanotubes guide oriented cell growth and promote electrophysiological homogeneity for synthetic cardiac tissues, Adv. Mater. 29 (44) (2017).
[22] M. Shevach, S. Fleischer, A. Shapira, T. Dvir, Gold nanoparticle-decellularized matrix hybrids for cardiac tissue engineering, Nano Lett. 14 (10) (2014) 5792–5796.
[23] Z. Cui, N.C. Ni, J. Wu, G.Q. Du, S. He, T.M. Yau, R.D. Weisel, H.W. Sung, R.K. Li, Polypyrrole-chitosan conductive biomaterial synchronizes cardiomyocyte contraction and improves myocardial electrical impulse propagation, Theranostics 8 (10) (2018) 2752–2764.
[24] T.H. Qazi, R. Rai, D. Dippold, J.E. Roether, D.W. Schubert, E. Rosellini, N. Barbani, A.R. Boccaccini, Development and characterization of novel electrically conductive PANI-PGS composites for cardiac tissue engineering applications, Acta Biomater. 10 (6) (2014) 2434–2445.
[25] R. Balint, N.J. Cassidy, S.H. Cartmell, Conductive polymers: towards a smart biomaterial for tissue engineering, Acta Biomater. 10 (6) (2014) 2341–2353.
[26] N. Saito, K. Aoki, Y. Usui, M. Shimizu, K. Hara, N. Narita, N. Ogihara, K. Nakamura, N. Ishigaki, H. Kato, H. Haniu, S. Taruta, Y.A. Kim, M. Endo, Application of carbon fibers to biomaterials: a new era of nano-level control of carbon fibers after 30-years of development, Chem. Soc. Rev. 40 (7) (2011) 3824–3834.
[27] K.A. Jockisch, S.A. Brown, T.W. Bauer, K. Merritt, Biological response to chopped-carbon-fiber-reinforced peek, J. Biomed. Mater. Res. 26 (2) (1992) 133–146.
[28] H. Luo, G. Xiong, Z. Yang, S.R. Raman, Q. Li, C. Ma, D. Li, Z. Wang, Y. Wan, Preparation of three-dimensional braided carbon fiber-reinforced PEEK composites for potential load-bearing bone fixations. Part I. Mechanical properties and cytocompatibility, J. Mech. Behav. Biomed. Mater. 29 (2014) 103–113.
[29] F. Wu, A. Gao, J. Liu, Y. Shen, P. Xu, J. Meng, T. Wen, L. Xu, H. Xu, High modulus conductive hydrogels enhance in vitro maturation and contractile function of primary cardiomyocytes for uses in drug screening, Adv. Healthc. Mater. 7 (24) (2018), e1800990.
[30] Y.X. Luo, X. Tang, X.Z. An, X.M. Xie, X.F. Chen, X. Zhao, D.L. Hao, H.Z. Chen, D.P. Liu, SIRT4 accelerates Ang II-induced pathological cardiac hypertrophy by inhibiting manganese superoxide dismutase activity, Eur. Heart J. 38 (18) (2017) 1389–1398.
[31] S.K. Ramadass, S. Perumal, A. Gopinath, A. Nisal, S. Subramanian, B. Madhan, Sol-gel assisted fabrication of collagen hydrolysate composite scaffold: a novel therapeutic alternative to the traditional collagen scaffold, ACS Appl. Mater. Interfaces 6 (17) (2014) 15015–15025.
[32] J.O. You, M. Rafat, G.J. Ye, D.T. Auguste, Nanoengineering the heart: conductive scaffolds enhance connexin 43 expression, Nano Lett. 11 (9) (2011 Sep 14) 3643–3648.
[33] X. Qian, J. Zhi, L. Chen, J. Zhong, X. Wang, Y. Zhang, S. Song, Evolution of microstructure and electrical property in the conversion of high strength carbon fiber to high modulus and ultrahigh modulus carbon fiber, Compos. Appl. Sci. Manuf. 112 (2018) 111–118.
[34] D.-H. Cho, S.-B. Yoon, C.-W. Cho, J.-K. Park, Effect of additional heat-treatment temperature on chemical, microstructural, mechanical, and electrical properties of commercial PAN-based carbon fibers, Carbon Lett. 12 (4) (2011) 223–228.
[35] C.W. Hsiao, M.Y. Bai, Y. Chang, M.F. Chung, T.Y. Lee, C.T. Wu, B. Maiti, Z.X. Liao, R.K. Li, H.W. Sung, Electrical coupling of isolated cardiomyocyte clusters grown on aligned conductive nanofibrous meshes for their synchronized beating, Biomaterials 34 (4) (2013) 1063–1072.
[36] Y. Liu, J. Lu, G. Xu, J. Wei, Z. Zhang, X. Li, Tuning the conductivity and inner structure of electrospun fibers to promote cardiomyocyte elongation and synchronous beating, Mater. Sci. Eng. C Mater. Biol. Appl. 69 (2016 Dec 1) 865–874.
[37] R. Schulz, P.M. Gorge, A. Gorbe, P. Ferdinandy, P.D. Lampe, L. Leybaert, Connexin 43 is an emerging therapeutic target in ischemia/reperfusion injury, cardioprotection and neuroprotection, Pharmacol. Ther. 153 (2015) 90–106.
[38] R.C. Addis, J.A. Epstein, Induced regeneration–the progress and promise of direct reprogramming for heart repair, Nat. Med. 19 (7) (2013) 829–836.
[39] S. Yamada, W.J. Nelson, Localized zones of Rho and Rac activities drive initiation and expansion of epithelial cell-cell adhesion, J. Cell Biol. 178 (3) (2007) 517–527.
[40] M. Noorman, M.A. van der Heyden, T.A. van Veen, M.G. Cox, R.N. Hauer, J.M. de Bakker, H.V. van Rijen, Cardiac cell-cell junctions in health and disease: electrical versus mechanical coupling, J. Mol. Cell. Cardiol. 47 (1) (2009) 23–31.
[41] X. Fan, C.J. Heijnen, M.A. van der Kooij, F. Groenendaal, F. van Bel, The role and regulation of hypoxia-inducible factor-1alpha expression in brain development and neonatal hypoxic-ischemic brain injury, Brain Res. Rev. 62 (1) (2009) 99–108.
[42] M. Giannotta, M. Trani, E. Dejana, VE-cadherin and endothelial adherens junctions: active guardians of vascular integrity, Dev. Cell 26 (5) (2013) 441–454.
[43] M.H. Mahmoudinezhad, A. Karkhaneh, K. Jadidi, Effect of PEDOT:PSS in tissue engineering composite scaffold on improvement and maintenance of endothelial cell function, J. Biosci. 43 (2) (2018) 307–319.
[44] D. Strassheim, E. Gerasimovskaya, D. Irwin, E.C. Dempsey, K. Stenmark, V. Karoor, RhoGTPase in vascular disease, Cells 8 (6) (2019 Jun 6) 551.
[45] J. Meng, Z. Han, H. Kong, X. Qi, C. Wang, S. Xie, H. Xu, Electrospun aligned nanofibrous composite of MWCNT/polyurethane to enhance vascular endothelium cells proliferation and function, J. Biomed. Mater. Res. 95 (1) (2010) 312–320.
[46] H.A. Owida, J.I. Al-Nabulsi, F. Alnaimat, M. Al-Ayyad, N.M. Turab, A. Al Sharah, M. Shakur, Recent applications of electrospun nanofibrous scaffold in tissue engineering, Appl. Bionics Biomechanics (2022 Feb 9), 1953861, 2022.
[47] S. Pok, F. Vitale, S.L. Eichmann, O.M. Benavides, M. Pasquali, J.G. Jacot, Biocompatible carbon nanotube-chitosan scaffold matching the electrical conductivity of the heart, ACS Nano 8 (10) (2014) 9822–9832.
[48] J. Zhou, J. Chen, H. Sun, X. Qiu, Y. Mou, Z. Liu, Y. Zhao, X. Li, Y. Han, C. Duan, R. Tang, C. Wang, W. Zhong, J. Liu, Y. Luo, M. Mengqiu Xing, C. Wang, Engineering the heart: evaluation of conductive nanomaterials for improving implant integration and cardiac function, Sci. Rep. 4 (2014) 3733.
[49] A.S.T. Smith, H. Yoo, H. Yi, E.H. Ahn, J.H. Lee, G. Shao, E. Nagornyak, M.A. Laflamme, C.E. Murry, D.H. Kim, Micro- and nano-patterned conductive graphene-PEG hybrid scaffolds for cardiac tissue engineering, Chem. Commun. 53 (53) (2017) 7412–7415.
[50] K. Zhu, S.R. Shin, T. van Kempen, Y.C. Li, V. Ponraj, A. Nasajpour, S. Mandla, N. Hu, X. Liu, J. Leijten, Y.D. Lin, M.A. Hussain, Y.S. Zhang, A. Tamayol, A. Khademhosseini, Gold nanocomposite bioink for printing 3D cardiac constructs, Adv. Funct. Mater. 27 (12) (2017), 1605352 pii.
[51] E. Frank, L.M. Steudle, D. Ingildeev, J.M. Sporl, M.R. Buchmeiser, Carbon fibers: precursor systems, processing, structure, and properties, Angew Chem. Int. Ed. Engl. 53 (21) (2014) 5262–5298.
[52] X. Huang, Fabrication and properties of carbon fibers, Materials 2 (4) (2009) 2369–2403.
[53] K. Cai, K. Yao, S. Lin, Z. Yang, X. Li, H. Xie, T. Qing, L. Gao, Poly(D,L-lactic acid) surfaces modified by silk fibroin: effects on the culture of osteoblast in vitro, Biomaterials 23 (4) (2002) 1153–1160.
[54] X. Hu, W. Liu, L. Sun, S. Xu, T. Wang, J. Meng, T. Wen, Q. Liu, J. Liu, H. Xu, Magnetic nanofibrous scaffolds accelerate the regeneration of muscle tissue in combination with extra magnetic fields, Int. J. Mol. Sci. 23 (8) (2022 Apr 18) 4440.
[55] K. Li, Y. Wang, Z. Miao, D. Xu, Y. Tang, M. Feng, Chitosan/gelatin composite microcarrier for hepatocyte culture, Biotechnol. Lett. 26 (11) (2004) 879–883.
[56] M. Zhang, B. Guo, Electroactive 3D scaffolds based on silk fibroin and water-borne polyaniline for skeletal muscle tissue engineering, Macromol. Biosci. 17 (9) (2017 Sep).
[57] L. Feng, J.D. Andrade, Protein adsorption on low temperature isotropic carbon: V. How is it related to its blood compatibility? J. Biomater. Sci. Polym. Ed. 7 (5) (1995) 439–452.
[58] M. Fedel, A. Motta, D. Maniglio, C. Migliaresi, Carbon coatings for cardiovascular applications: physico-chemical properties and blood compatibility, J. Biomater. Appl. 25 (1) (2010 Jul) 57–74.
[59] J. Meng, H. Kong, H.Y. Xu, L. Song, C.Y. Wang, S.S. Xie, Improving the blood compatibility of polyurethane using carbon nanotubes as fillers and its implications to cardiovascular surgery, J. Biomed. Mater. Res. 74 (2) (2005 Aug 1) 208–214.
[60] L.P. da Silva, S.C. Kundu, R.L. Reis, V.M. Correlo, Electric phenomenon: a disregarded tool in tissue engineering and regenerative medicine, Trends Biotechnol. 38 (1) (2020 Jan) 24–49.
[61] Q. Zhao, J. Wang, H. Cui, H. Chen, Y. Wang, X. Du, Programmed shape-morphing scaffolds enabling facile 3D endothelialization, Adv. Funct. Mater. 28 (29) (2018), e201801027.